ELSEVIER

Journal of Nuclear Materials 295 (2001) 133–148

journal of nuclear materials

www.elsevier.nl/locate/jnucmat

Review

The fractal nature of the surface of uranium dioxide: a resolution of the short-lived/stable gas release dichotomy

R.J. White [1]

OECD Halden Reactor Project, P.O. Box 173, N-1751 Halden, Norway

Received 29 November 2000; accepted 31 March 2001

Abstract

The framework for analysis of fission product release in the Halden gas flow rigs has been developed over a period of 20 years. The predominant mode of release is single gas atom diffusion to free surfaces with a small, but burn-up-dependent contribution from direct recoil. Measurements of longer-lived fission products indicated that their release appeared to be controlled by a diffusion coefficient, which, at low temperatures, was several orders of magnitude smaller than that of the shorter-lived fission products. The enhanced release of the shorter-lived products was attributed to a near-surface enhancement effect. However, a theoretical study of a two-zone diffusion model reveals that it is incapable of accounting for the observations. A model based on the fractal nature of the uranium dioxide surface circumvents these difficulties and provides a framework in which a single three-term diffusion coefficient can be used to describe the release of both short- and long-lived fission products.

1. Introduction

The release of fission gas from irradiated UO_2 plays a key role in the performance and stability of reactor fuel. Two particular areas are of interest, namely, the effects of stable fission gases on the thermal and dimensional performance and the radiological aspects of the unstable fission products. For these reasons a physical understanding of the various aspects of the release processes is preferred over a purely empirical description.

The measurement of fission gas release in test rods is an important prerequisite to the mathematical modelling of the release process and has been an integral part of the Halden Project Joint Programme for many years. Experimental techniques range from the use of diaphragm and bellows pressure transducers for the in-pile monitoring of the pressure caused by release of stable fission gases, post-irradiation examination of end-of-life gas releases as well as the on-line monitoring of radioactive fission gases via gamma spectrometry in the so-called gas flow rigs. There have been a number of findings over the years but perhaps of most importance has been the establishment of the fission gas release threshold which relates the burn-up for the onset of significant stable gas release with the peak fuel centre temperature. This was achieved through the use of both in-pile and PIE studies [1]. More recently the gas flow rigs have enabled careful experiments to be performed to elucidate details of the release processes of both the radioactive and the longer-lived fission gases.

2. Experimental perspective

2.1. The Harwell swept capsule experiments

The predominant mode of fission gas release occurs through the atomic diffusion of single gas atoms to free surface and grain boundaries. The rate at which gas atoms diffuse in UO_2 is therefore of fundamental importance for the understanding of the processes involved. A series of definitive experiments was performed by Turnbull et al. [2] during the late 1970s and early 1980s in which large single crystals and polycrystals of UO_2 were irradiated in the Swept Capsule Rig at

E-mail address: fuelrod@btinternet.com (R.J. White).

[1] Present address: 18, Green Close, Uley, Dursley, Gloucestershire GL 11 5TH, UK.

0022-3115/01/$ - see front matter
PII: S0022-3115(01)00571-2

UKAEA laboratories at Harwell in the UK. By collecting the released fission products on a cold-finger, Turnbull and his co-workers were able to calculate the fission gas diffusion coefficient as a function of fission rating and temperature. The usual difficulty involved in interpreting such data relates to the value of the fuel surface-to-volume ratio (S/V), or its equivalent, the radius of the equivalent diffusion sphere. In these experiments the surface areas of the single crystals were measured with optical microscopy and so the data provide absolute values of diffusion coefficients covering the temperature range from 250°C to 1400°C.

Turnbull's data [2,3] could be understood on the basis of a diffusion coefficient comprising three separate components, as follows:

$$\begin{aligned} &D = D_1 + D_2 + D_3 \quad \mathrm{m^2/s} \\ &\text{with} \\ &D_1 = 7.6 \times 10^{-10}\, \mathrm{e}^{-35000/T_\mathrm{K}}, \\ &D_2 = 3.22 \times 10^{-16}\, W^{1/2}\, \mathrm{e}^{-13800/T_\mathrm{K}}, \\ &D_3 = 6 \times 10^{-23}\, W, \end{aligned} \tag{1}$$

where T_K is the absolute temperature and W is the mass rating in W/gU.

At the highest temperatures an intrinsic thermally activated process appears to dominate, although the origin of this is not fully understood. It seems likely that the mechanism is one of atomic diffusion through the cation lattice by means of thermally activated vacancies. The contribution (D_1) has a temperature dependence similar to that reported by Davies and Long [4] although the pre-exponent is now thought to be an order of magnitude greater than in Eq. (1). Below 1400°C, Turnbull [2] concludes that diffusion occurs by means of a vacancy supersaturation, following the loss of irradiation produced vacancies and interstitials to fixed sinks under mutual recombination dominant conditions. This term (D_2) depends on temperature and the square root of the fission rating. The final contribution to the diffusivity is the athermal, rating-dependent, tail and no firm conclusions emerge as to the mechanism. Turnbull follows Matzke [5] in adopting a term proportional to the fission rate and scaled to agree with the low temperature plateau.

2.2. The Halden gas flow rigs

It was realised at the outset that the gas flow rigs employed at the OECD Halden Reactor Project in Norway [6] could not address the issue of absolute determination of diffusion coefficients. Instead, the design philosophy focused on the role of obtaining high quality fission product release data during the operation of integral fuel rods. A principal target was the acquisition of data on the radioactive isotopes of iodine, which play an important role in the safety cases for reactor operations in many countries. In addition, information on the evolution of the short-lived fission product releases with irradiation, associated with changing fuel microstructures was also seen as a desirable goal.

The release rates of short-lived fission products are usually defined in terms of the ratio of the release rate, R, to the birth rate, B. For small R/B ratios, typically less than 10%, Booth [7] has shown that under steady-state conditions, the release-to-birth rate ratio from a spherical grain of radius 'a' is approximately given by

$$\frac{R}{B} = \frac{3}{a}\sqrt{\frac{D}{\lambda}}, \tag{2}$$

where D is the diffusion coefficient and λ is the decay constant of the isotope under consideration. This is usually generalised for non-spherical diffusion geometries by replacing the $3/a$ by S/V where S is the surface area and V is the volume of the specimen. The value of S/V provides information on the state of the fuel microstructure and reaches values of the order of 20–50% of the limiting value of $3/a$ particularly following extensive interlinkage of grain boundary porosity. In contrast, at the beginning of life, the S/V adopts values which are a small multiple of the geometric value, reflecting the presence of small cracks and open porosity in the as-sintered pellets.

For temperatures below about 700°C, the diffusion coefficient given in Eq. (1) is essentially temperature-independent and varies linearly with the fission rating. This was felt to be an ideal scenario for the study of microstructural changes in the gas flow rigs because, for reasonable values of fuel rating, typically below 25 kW/m, the average diffusion coefficient in the fuel will be independent of the temperature profile. Because of the weak dependence on temperature below 900°C it was also felt that rod-average diffusion coefficients could be obtained by integrating Eq. (1) with respect to temperature and rating across the radial and axial profiles of an operating rod. Additional confidence in this approach was provided by the in-pile measurement of the fuel centre temperature in these rigs, enabling a fuel modelling code to be tuned to the actual measured temperatures. An important additional feature of this integration process was that Eq. (1) could then be solved to provide a rod-average temperature corresponding to the rod-average diffusion coefficient [6].

Under operating conditions, a sweep gas, such as helium or argon, could be flushed through the fuel rod and the exiting gas routed past a gamma spectrometer. A variety of techniques were used to obtain measurements of gas release. The first involved the measurement of the activity of the gas as it flowed past the spectrometer and this provided estimates for fission products with half-lives less than 5 h, such as ^{137}Xe, ^{138}Xe, ^{139}Xe,

^{85m}Kr, ^{87}Kr, ^{88}Kr, ^{89}Kr and ^{90}Kr. In addition, the released gas could be trapped in the pipe in front of the spectrometer and the very short-lived products allowed to decay. An extended count could then be used to provide improved estimates of the longer-lived products with half-lives greater than 14 min, for example, ^{138}Xe, ^{87}Kr, ^{88}Kr and ^{85m}Kr. Finally, cold-trap techniques were employed to establish the release rates of the isotopes such as ^{131}I, ^{133}Xe, ^{131m}Xe and ^{85}Kr with half-lives varying from days to years. Turnbull et al. [8] have demonstrated that ^{85}Kr with a 10.72 year half-life can be used to estimate the stable fission gas release.

Tempest [9] has examined the measurement uncertainties involved in the fission product measurement scheme and also studied the repeatability of measurements. His conclusions are that the compounded uncertainties indicate that the release rates may be estimated to be within ±40%. Experiments performed under steady-state conditions suggest that the repeatability is nearer to ±20%. However, by far the largest area of uncertainty, and one not considered in Tempest's analysis, involves the sweeping efficiency. Under very high power conditions a large fraction of the released fission products will be retained in the fuel by thermal-expansion-induced stresses that cause crack closure and reduce the intra-rod communications. For this reason, the most reliable data have been obtained under low power conditions with large open fuel–clad gaps.

2.3. Analysis of the gas flow rig data: diffusional release

Eq. (2) was initially used in the analysis of the short-lived fission product release measured in the Halden gas flow rigs. However, even at low burn-ups it was evident that on the standard plots of $\ln(R/B)$ versus $\ln(\lambda)$ there was some flattening – see Fig. 1 – at the short-lived fission product end of the graph, whereas Eq. (2) indicates that a slope of −1/2 should operate for all fission products. This has been interpreted as arising from the recoil release, which is half-life-independent or lambda-independent. Recoil release arises because the energy released in the fission process – 200 MeV – is carried as kinetic energy by the recoiling fission fragments and the dissipation of this energy by the UO_2 lattice results in fission fragment ranges of around 6 μm [10]. If a fission event takes place within this distance of a free surface there is a strong possibility that the recoiled atom may be released directly. For this reason all subsequent analysis has treated the release as being described by

$$\left.\frac{R}{B}\right|_{\text{total}} = \left.\frac{R}{B}\right|_{\lambda\text{-independent}} + \frac{S}{V}\sqrt{\frac{\alpha D}{\lambda}}, \tag{3}$$

where the diffusional release component is modified by the inclusion of α which accounts for any precursor

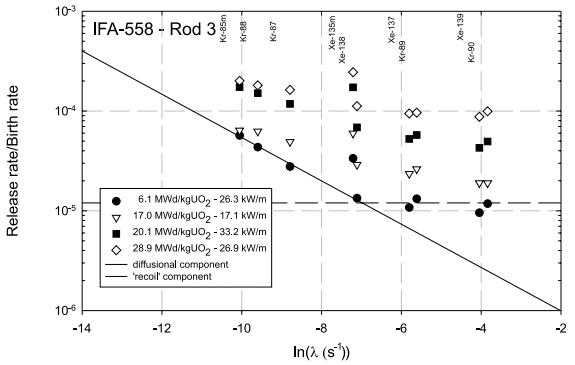

Fig. 1. Fission product release-to-birth rate ratios (R/B) against decay constant, λ, for rod 3 of the IFA-558 gas flow rig at four different burn-ups. The solid line shows the expected slope of the diffusional release component. Note the increase of the lambda-independent component with increasing burn-up.

enhancement effects [11]. The R/B values have therefore been fitted to an equation of the form

$$\left.\frac{R}{B}\right|_{\text{total}} = A + C\sqrt{\frac{\alpha}{\lambda}}. \tag{4}$$

In Eq. (4), A can be identified with the lambda-independent component in Eq. (3). Similarly, C is referred to as the diffusional slope and is equal to $S\sqrt{D}/V$. Eq. (4) has been used in conjunction with the rod-average diffusion coefficient obtained from integration of Eq. (1) using the UK fuel modelling code, MINIPAT [12], to obtain through-life estimates of the evolution of the S/V [6]. These experiments clearly indicate the onset of major microstructural changes such as grain boundary interlinkage [13] when the S/V may increase from values of around 10^4–10^5 m^{-1}.

In addition, tests on rods of the Instrumented Fuel Assembly, IFA-504, involving the cold trapping of longer-lived fission products, were analysed using the standard Booth equations for stable gas release [14] in conjunction with values of S/V obtained from the analysis of the short-lived fission products [6,15]. It was expected that the derived diffusion coefficients would confirm the formulation used in the calculation of the rod-average diffusion coefficient but this was not the case. The evaluations are displayed in Fig. 2 along with later estimates from ramps on IFA-430 [16] and IFA-504 for the short-lived products as well as values of rod-average diffusion coefficient obtained from the ^{131}I release measurements. Unless a specific isotope is stated in the legend, all of the short-lived fission product data were obtained under steady-state or quasi-steady-state conditions using flow spectrometry to obtain isotopic releases of the whole range of xenon and krypton isotopes mentioned in Section 2.2.

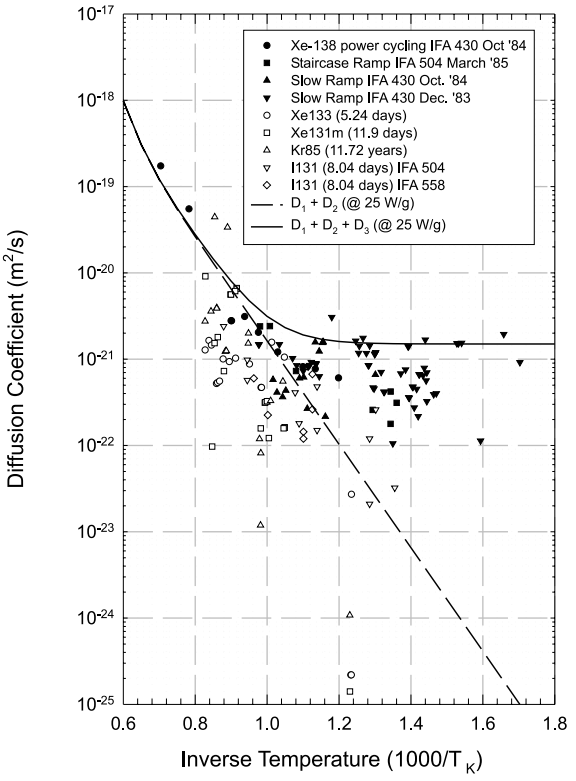

Fig. 2. Fission product diffusion coefficients measured in the gas flow rigs in Halden. The solid symbols are for short-lived fission products and the open symbols for the longer-lived species. Note the apparent enhancement of short-lived products over their longer-lived counterparts at low temperatures. The lines represent the two-term and the three-term diffusion coefficients. Unless otherwise stated all evaluations are based on the diffusional slope analysis of Eq. (4) utilising a range of at least six fission products.

In all of these cases the temperature axis is obtained by evaluating the rod-average temperature equivalent to the rod-average diffusion coefficient appropriate to the actual conditions operating in the fuel rod. As mentioned earlier, most of these tests were conducted in regions where the temperature dependence of the diffusion coefficient was weak and the rod-average value was controlled by the D_3 term. There are uncertainties associated with this procedure but it should be emphasised that the value of the S/V was obtained by using a rod-average value of diffusion coefficient so the comparison is between two values of diffusion coefficient and the discrepancy exists regardless of where on the temperature axis the data are plotted.

There are a number of points to be made about the cold-trap experiments reported above. In all cases, cold trapping was performed after the reactor had been shut down after a lengthy period of steady-state operation thereby avoiding any complications caused by transient release. Under these conditions there is no problem flushing the rods as the fuel–clad gap is large and the sweeping efficiency is nearly 100% so the amount of gas collected should exceed that obtained during flushing at-power. Secondly, the rods under consideration had been sealed to allow the accumulation of the fission gases and in most cases a burn-up increment of around 1 $\mathrm{MWd/kgUO_2}$ had accumulated so the amount of gas in the cold trap was easily measurable. Finally, each trap was measured a number of times at intervals to ensure consistency of results as well as to ensure that no leakage had occurred during storage.

As would be expected from this type of analysis there is a significant amount of scatter to the data. What is very clear, however, is the way the data split into two sets at low temperatures. The upper branch describing the short-lived releases and the lower branch describing the long-lived products. Also shown in Fig. 2 are the calculations for $D_1 + D_2 + D_3$ and the $D_1 + D_2$ obtained from Eq. (1) and this comparison led to the inference that the short- and long-lived products diffused at different rates.

On an atomic level it is difficult to conceive how the diffusion rates of short- and long-lived fission products can be different. At higher temperatures, fission gas atoms may be trapped in intra-granular fission gas bubbles [17]. These bubbles are formed in the wake of passing fission fragments and also destroyed by fission fragments [18] by a process of irradiation-induced re-solution. Speight [19] has shown theoretically how a dynamic balance may be set up between nucleation, diffusional growth and destruction and how this may affect the bulk diffusion coefficient. A process such as this might be expected to lead to a lower diffusion coefficient for stable gas atoms where residence time in bubbles is important whereas for shorter-lived products the radioactive decay process dominates over short-term trapping. There are two problems with such an approach. The first is that significant bubble growth is only observed at temperatures in excess of 1300°C [17] whereas these experiments were conducted at temperatures below 1000°C. Secondly, recent transmission and scanning electron microscopy studies of intra-granular bubble growth [20,21] cast doubt on whether most of the features are even bubbles. The bubbles observed at around 800–1000°C occur at concentrations of 1–2×10^{24} $\mathrm{m^{-3}}$ with diameters of around 1 nm [17,20]. Transients to higher temperatures indicate that only about 1 in 10^4 of these bubbles grow and the concentrations are further reduced to around 10^{19} $\mathrm{m^{-3}}$ by irradiation-induced re-solution. The growth process provides a potent source of transient fuel swelling but the low density of growing bubbles means that the attenuation of the diffusion coefficient is much lower than

previously thought [19] as well as being of a transient nature.

The argument was eventually rationalised by proposing that the diffusion coefficient of all fission products was the same, that is $D_1 + D_2$, and that the D_3 term only operated a short distance from the fuel surface thereby only affecting the short-lived products. In order to explain the differences between the short-lived and long-lived products this layer of enhancement needed to be of the order of 10–20 nm thick [8,15].

2.4. Analysis of the gas flow rig data: recoil release

The other component of release in Eqs. 3 and 4 has been called recoil release or the lambda-independent component of release. Many experiments have been performed to elucidate the actual release mechanism involved. Early tests involving IFA-504 and high-pressure [22] argon fill gas demonstrated that the measured release was sensitive to the stopping power of the sweep gas. For example, in those tests on low burn-up fuel, the normal measured value of this component was less than 5×10^{-5} with low-pressure helium whereas it rose to values in excess of 2×10^{-4} with 30 bar argon. This was interpreted on the basis that the recoils not stopped by the helium implanted themselves into the cladding whereas, with higher density argon, the recoils would be stopped and swept to the gamma spectrometer.

The higher value of $2–3 \times 10^{-4}$ was taken as the maximum possible value of recoil release but as burn-up accumulated, the baseline value with helium fill gas appeared to increase steadily as well. Since the range of fission fragments in helium fill gas is of the order of 50–100 μm, it was thought that the recoil release should decrease as the fuel–clad gap decreased and that the only source of recoils would arise from the outer geometric surface of the fuel thus precluding any strong effect from recoils released into newly developed porosity, this having dimensions of the order of μm or less. The experimental evidence pointed firmly in the opposite direction and detailed tests of the pressure sensitivity with helium fill gas were performed both before and after interlinkage to establish the nature of the release. The results of these tests are shown in Fig. 3 and demonstrate that the pressure sensitivity shows little change with burn-up [13]. It must therefore be concluded that only the pressure-dependent component of the lambda-independent release arises from recoils. An additional curve has been added to Fig. 3 showing the pressure dependence with argon at high burn-ups and this shows a tendency to saturate at high pressures indicating a maximum possible recoil release of $2–3 \times 10^{-4}$, a value little changed from that measured in argon at low burn-ups thus confirming that the actual recoil release is unchanged. At high burn-ups this leaves a large lambda-independent component at zero pressure where all the recoils would be expected to embed themselves into structural parts of the cladding. This component must arise from some mechanism other than recoil.

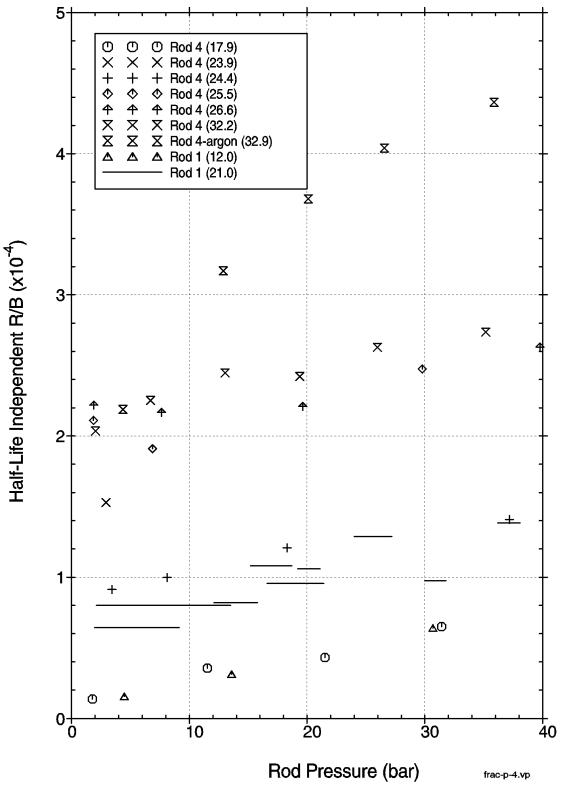

Fig. 3. Variation of the lambda-independent component of the short-lived fission product release with rod pressurisation in IFA-504 with burn-up ($MWd/kgUO_2$). It is thought that the pressure-dependent part results from recoiled fission fragments being stopped by the sweep gas. Note that the intercept or zero-pressure component increases with burn-up.

Very few candidates have been proposed. One suggestion was made by the author in 1985 [6] and was referred to as the release from the fissioning of sputtered uranium (FSU) on the basis that recoiling fission fragments would knock uranium dioxide fragments from the fuel; these could later undergo fission and their small size would mean that all fission gas atoms would escape regardless of half-life. While this process is likely to happen it is not likely to happen to the extent necessary to provide releases in excess of 2×10^{-4} and best estimates would suggest that the FSU value [6] is likely to be at least an order of magnitude less than the observed values.

A second suggestion came from Tempest in 1989 [13] who proposed that the fission gas diffusion coefficient was further enhanced very close to the surface giving rise to a directed diffusional flux rather than

random migration. This suggestion has never been examined in detail but is actually a further refinement of the argument that led to the adoption of the enhanced D_3 term in the near-surface layers [6,15]. In this case one might expect D_3 to increase progressively towards the fuel surface thus enhancing the products with the shortest diffusion fields preferentially over those with longer diffusion paths. This would then be expected to produce the enhanced values of release of the shortest-lived fission products. Tempest's proposal correctly interprets the pressure-dependent component as true recoil [13] and suggests that the zero pressure intercept is actually diffusional release but with a diffusion coefficient falling off with distance away from the surface such that the half-life dependence of Eq. (3) is nullified.

2.5. A summary of the problem

1. The release rates of short-lived fission products have been measured under regimes in which the diffusion coefficient is believed to be essentially athermal. The measurements can be understood by assuming that the releases comprise two components. The first, referred to as the diffusional component depends on the fission product half-life, while the second component, the recoil component is lambda-independent.
2. The fuel microstructure parameter, S/V, has been determined using the Turnbull [2,3] recommendations for diffusion coefficient in conjunction with Eqs. (3) and (4).
3. The release rates of longer-lived fission products have been determined by collecting the gas released over complete reactor cycles in liquid nitrogen-cooled charcoal-filled cold traps. (Note that the Halden HBWR is a test reactor and the cycles are much shorter than for a commercial reactor.)
4. Analysis has been performed using either Eqs. (3) and (4) for the ^{131}I, ^{131m}Xe and ^{133}Xe releases or the Booth equation for stable gas release [14] for ^{85}Kr. The value of S/V used in the analysis is equal to that derived from analysis of the short-lived fission products in adjacent reactor operating periods.
5. The value of the fission gas diffusion coefficient obtained from the longer-lived products is much smaller than that used for the analysis of the short-lived products.
6. The low-pressure, lambda-independent component of the short-lived fission gas release appears to increase with burn-up from a value of $2–5 \times 10^{-5}$ at the start-of-life to around 2×10^{-4} at 20 MWd/kgUO$_2$.
7. The pressure dependence of the lambda-independent component appears to remain constant with burn-up.

An illustration of some of the difficulties can be seen in Fig. 4, which shows the evolution of recoil and diffusional release components from a slow-ramp conducted

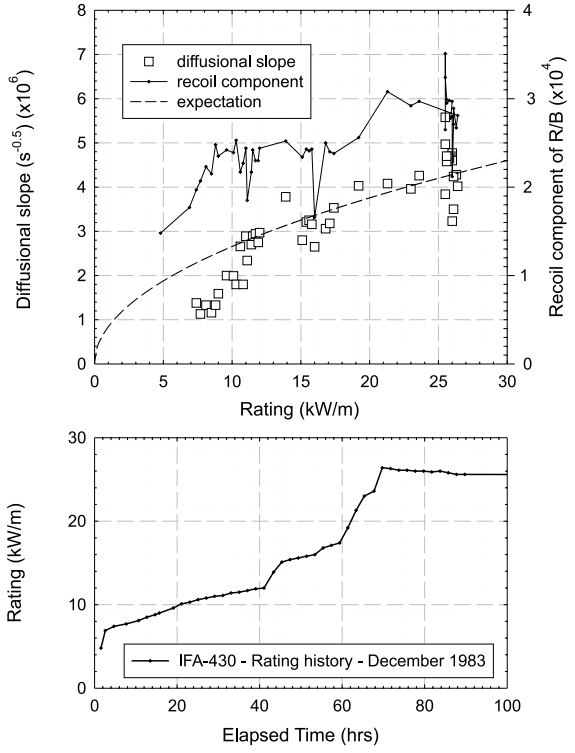

Fig. 4. Analysis of the slow-ramp in IFA-430 using standard diffusional analysis as in Eq. (4). The open symbols are the diffusional slope and the solid line is the lambda-independent component. Note that the magnitude of the diffusional slope falls below expectations based on a rating-dependent D_3 component. Note also the comparable increases of the two release components during the ramp.

on the IFA-430 assembly. The power history during the slow-ramp is shown in the lower trace and this was arranged so that the fission products measured were in diffusional/radioactive equilibrium. The transient solution of the diffusion equation contains an error function time dependence [23] and the approach to equilibrium takes around three half-lives. By the time the power reaches 10 kW/m all products with half-lives less than that of ^{85m}Kr (4.45 h) should be in equilibrium and the slow-ramp rate ensures that equilibrium will be maintained thereafter. The upper trace shows that both the recoil and diffusional release components increase with power in similar fashion. Also plotted on the upper trace is the expected trend of the diffusional release component for the rod-average diffusion coefficient given in Eq. (1). The measured values fall below expectations until the rating reaches 12 kW/m suggesting that D_3 is temperature-dependent. The failure to follow expectations cannot be attributed to non-equilibration because this power is only achieved after 42 h giving ample time for ^{85m}Kr equilibration.

The data in Fig. 4 have been used to evaluate the fission gas diffusion coefficient by scaling the required S/V so that the values coincide with the Turnbull equation [2] at 727°C. This is similar to the technique adopted by Turnbull to normalise the results from polycrystalline specimens to those obtained from his reference single crystals.

3. Two-zone diffusion

In order to test the two-zone diffusion hypothesis, the diffusion equation has been solved under the configuration depicted in Fig. 5. For simplicity, the steady-state diffusion equation shown below in Eq. (5) is considered.

$$D\nabla^2 c + \beta - \lambda c = 0. \tag{5}$$

This is solved in two zones for steady-state conditions. In the inner zone the diffusion coefficient takes the value D_i while in the outer region it takes the value D_o with $D_o > D_i$. At the interface between the two regions it is necessary to set the flux entering the interface equal to the flux leaving it otherwise there will be an accumulation of fission products. This is given by

$$D_i \left.\frac{\partial c}{\partial r}\right|_{\text{arriving}} = D_o \left.\frac{\partial c}{\partial r}\right|_{\text{leaving}}. \tag{6}$$

Eqs. (5) and (6) have been solved under a range of conditions using a finite difference method incorporating a geometrical series spatial mesh in the inner zone and linear mesh in the thin outer shell for maximum accuracy and minimal running time. Three-point discretisations have been used and a standard naive Gaussian elimination method applied to the tri-diagonal matrix. The values of R/B were obtained using two separate methods. The first employed a simple three-point gradient evaluation at the grain surface (divergence) and the second employed volume integration. Since the two methods are proven mathematically identical via Gauss's theorem it is reassuring to report that they also apply to computer simulations. It was also demonstrated that the Booth solutions could be reproduced under the trivial conditions of uniform diffusivity throughout.

The solutions have been obtained using a diffusion sphere radius equivalent to the S/V measured during the period when the cold-trapping data were obtained, that is, $S/V \approx 25\,000\ \text{m}^{-1}$. Similarly, the diffusion coefficients for the two zones are taken to be $D_1 + D_2$ and $D_1 + D_2 + D_3$ from Eq. (1). The results of the evaluations are summarised in Fig. 6 and demonstrate that the release of the longer-lived ^{133}Xe isotope is predominantly controlled by the diffusion rate in the outer zone. Thus the behaviour summarised in Fig. 2 cannot have arisen from diffusion in a two-zone model of the type modelled in Fig. 5 unless the short-lived and long-lived products had different diffusion rates.

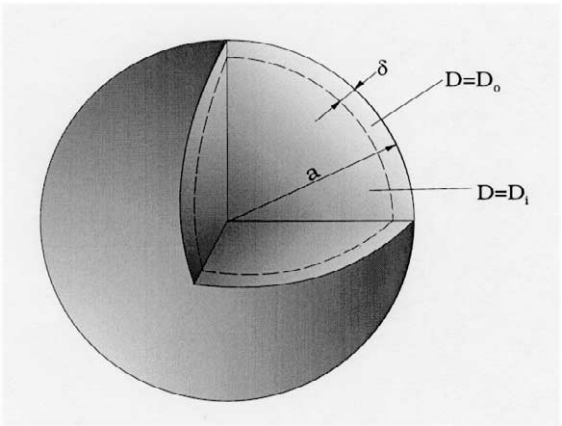

Fig. 5. Idealised geometry assumed for two-zone diffusional release calculations. The diffusion coefficient in the outer layer is much greater than that in the grain centre.

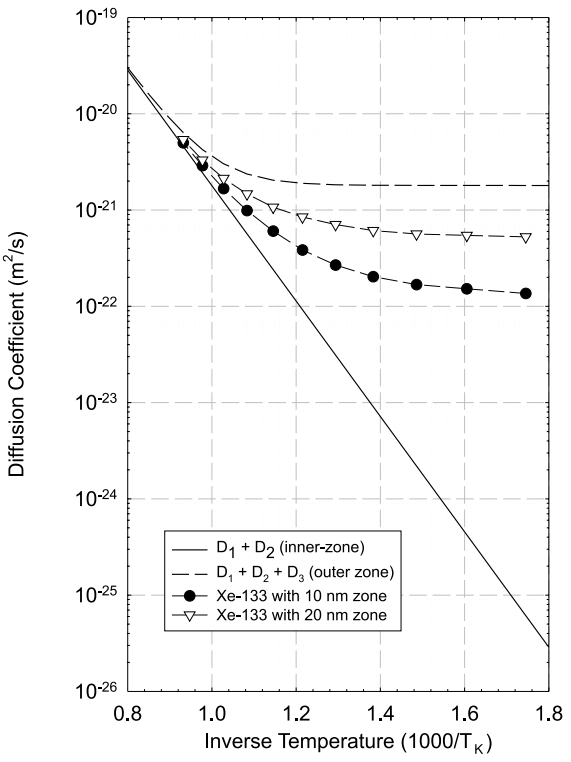

Fig. 6. Predictions of ^{133}Xe (5.24-day half-life) release assuming two-zone model with inner-zone diffusivity equal to $D_1 + D_2$ and outer-zone diffusivity equal to $D_1 + D_2 + D_3$. The predictions are equated to the effective diffusion coefficient for equivalent release and are calculated for two values of the zone thickness.

It must therefore be concluded that the proposals made in 1984 [6,15] for the solution of the short-lived/long-lived dichotomy and resurrected/extended in 1989 [13] to explain the increase in the lambda-independent release fail to account for the observations and that, regardless of the degree of enhancement in the surface layers, the long-lived products would always appear to diffuse at that rate if the temperature was decreased sufficiently.

4. An alternative solution to the problem

4.1. Random fractals

Since there is a distinct lambda-dependent component to the measured short-lived fission product releases it is clear that the release is controlled by the diffusion of gas atoms to the grain boundaries or free surfaces. However, the difference between the release of stable atoms and the release of very short-lived products requires an explanation and, from the simulations presented in the previous section it is evident that the solution does not involve spatially varying diffusion coefficients since in the limit of slow diffusion, i.e. low temperatures, all release is controlled by the diffusion coefficient in the very-near-surface layer. The bifurcation in the derived diffusion coefficient plot becomes more extreme at low temperatures whereas the spatially varying diffusion coefficient approach indicates it should become less severe. An examination of Eq. (3) reveals that the only alternative variable in the Booth release equation is the S/V and the possibility of this being a function of fission product decay constant has always been ignored.

However, the variation of linear and surface properties with scaling is well known in a variety of fields. This self-similarity is referred to as random fractal behaviour to distinguish it from the regular fractal behaviour exhibited by such fractals as the Koch Snowflake or the Cantor Set [24,25]. The self-similarity is revealed over a range of magnifications and, in general, the measured parameter increases as the size of the measuring stick is reduced. There are, of course, limits to this behaviour, which will be reached when the measuring stick approaches the dimensions of the atomic spacing. At the other extreme, the measured parameter must also have a minimum value appropriate to the gross structural dimensions of the body.

A possible solution to the stable/unstable gas release dichotomy could be found if the surface of UO_2 exhibited fractal behaviour at small dimensions of the order of the diffusion length of the short-lived fission products.

4.2. What yardstick can be used to measure fuel surface areas?

It should be possible, in principle, to measure the surface area under different magnifications in the scanning electron microscope. However, of more value is the possibility that the fission products themselves can be used as microscopic measuring devices. For a fission product with decay constant, λ, and diffusion coefficient, D, the mean-diffusion distance travelled, that is, the random walk distance, between creation and decay is of the order of

$$\delta \approx \sqrt{\alpha D t_{\text{life}}} \approx \sqrt{\frac{\alpha D}{\lambda}}, \tag{7}$$

where α takes account of the precursor enhancement effects [11]. A typical value of the rod-average diffusion coefficient at 20 kW/m is 10^{-21} m^2/s and a fission product with a half-life of around 5 min has $\lambda = 2 \times 10^{-3}$ s^{-1} which gives a diffusion distance of 0.7 nm, that is, around two lattice spacings. This kind of dimension would be typical of the stacking ledges which appear on growing crystals so surface features of this scale should not be ruled out. In fact, using the concept of the diffusion distance in Eq. (7), the Booth release equation may be redrafted to the form

$$\frac{R}{B} = \frac{S}{V}\delta, \tag{8}$$

which makes it clear that the release to birth rate ratio is equal to the ratio of the volumes of the surface shell of thickness equal to the diffusion distance, δ, of the isotope under consideration to the volume of the entire solid.

An example of how the surface area might appear to increase with decreasing diffusion distance is shown in Fig. 7 which idealises a section of the surface as a regular fractal like the Koch Snowflake [24]. Each successive magnification of this structure shows exactly the same level of detail and it can be seen that the diffusion distance can be viewed as a 'measuring rod' with which to examine the detailed surface morphology. Since the ideal surface has this appearance regardless of magnification, the probing effects of a fission product are identical at all levels of decay constant. For very small diffusion distances this shell volume faithfully follows the contours of the surface. The effective surface area is the volume within the diffusion distance of the surface divided by the diffusion distance so, as this distance increases, the effects of surface undulations decrease, and the effective surface area decreases accordingly. For the simple example presented here a radioactive fission product effectively samples surface features with wavelength and amplitude around five to ten times its own diffusion

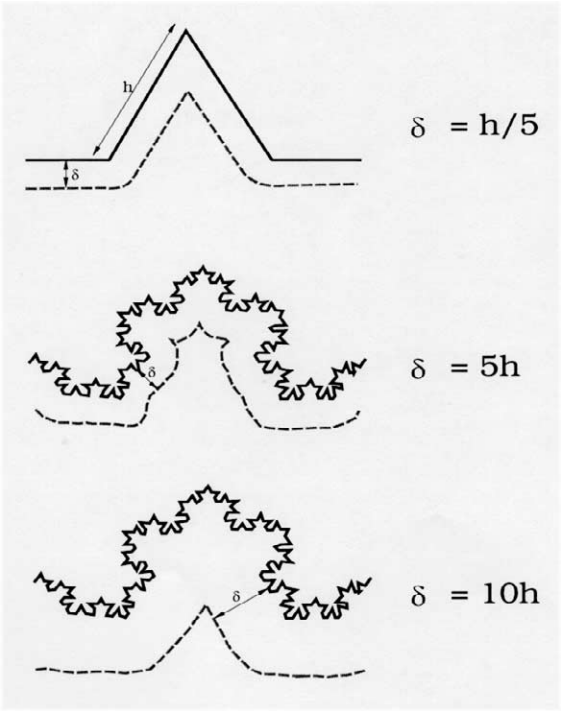

Fig. 7. The Koch Snowflake fractal. The diffusion distance explores the detail of the fractal. A very much larger surface area is available for the release of short-lived fission products.

distance. At distances greater than this the details of the surface features have essentially disappeared.

The standard method of quantification of the fractal nature of an object is to measure how many boxes of side length, δ, are required to cover it [26]. The method can therefore be used for either line segments, such as coastlines, or surface areas, such as fracture surfaces. The parameter defining the fractality is the box-counting dimension, D_B. The box-counting dimension [26] is defined in terms of the number of boxes, $N(\delta)$ required to cover the object, as follows:

$$D_B = \frac{\ln(N(\delta))}{\ln(1/\delta)}. \tag{9}$$

The box-counting dimension, D_B, is closely related to the Hausdorff dimension [24,25]. If D_B equals 2 the surface is not a fractal; a fractal is an object whose box-counting or Hausdorff dimension is greater than its topological dimension and for a surface the topological dimension is 2.

The surface area, $S(\delta)$ for any given box size is equal to $N(\delta)\delta^2$ so the release in Eq. (8) may be rewritten as

$$\frac{R}{B} = \frac{\delta_0^{D_B}}{V}\delta^{3-D_B} = S_F\delta^{3-D_B}, \tag{10}$$

where δ_0 is a reference value of mean-diffusion distance for scaling purposes. For the trivial case where the surface is non-fractal, the box-counting dimension, D_B, is equal to 2, i.e. the topological dimension, and Eq. (10) reduces to the standard Booth form.

It is not immediately possible to test this approach because of the absence of information on the diffusion coefficient. Alternatively, the diffusion coefficient can be ignored for the time being, on the basis that for any particular set of data it remains constant and the analysis may be performed in terms of a fractal pseudo-box size, δ_p, where

$$\delta_p = \sqrt{\frac{\alpha}{\lambda}} = \frac{\delta}{\sqrt{D}}. \tag{11}$$

Thus manipulation of the Booth equation provides the following release equation:

$$\frac{R}{B} = \frac{\delta_p^3}{V}\left(\frac{\delta_0}{\delta_p}\right)^{D_B} D^{(3-D_B)/2} = S_{PF}\delta_p^{3-D_B}. \tag{12}$$

To examine the fractality of the UO_2 surface it is necessary to study the dependence of the S/V on the fission product mean-diffusion distance, δ, and this can be effected by rearranging the Booth release equation – Eq. (8) – to form

$$\frac{S}{V} = \frac{R}{B}\left(\frac{1}{\delta}\right). \tag{13}$$

A plot of the right-hand side of Eq. (13) against δ should be a horizontal line if the surface is non-fractal while a negative slope would indicate that the fuel surface area depended on the fission product mean-diffusion distance and was of a fractal nature.

4.3. Pseudo-fractal behaviour in IFA-558

This approach has been tested on the data from rod 3 of IFA-558. This rod has been chosen because the pressures were maintained at a low value throughout the experiment thereby precluding enhanced values of true recoil release. The results of a number of measurements taken both prior to and following the interlinkage threshold are shown in Fig. 8 demonstrating a clear fractal type dependence over several orders of change in the pseudo-box size parameter, $\delta_p = \sqrt{(\alpha/\lambda)}$, with the box-counting dimension, D_B, taking values between 2 and 3. It should be noted that these are the same data that were used in Fig. 1.

At this stage the analysis should be referred to as pseudo-fractal because the scaling parameter is not a true dimension. This only becomes dimensional when the diffusion coefficient is included in the analysis although the inclusion of the diffusion coefficient will not lead to a change in D_B or to the conclusion that the

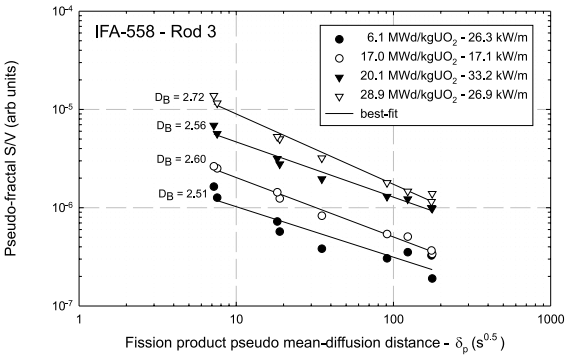

Fig. 8. Pseudo-fractal plot for rod 3 of IFA-558, which illustrates the strong dependence of the pseudo-S/V on the fission product diffusion distance. The data here are the same as those in Fig. 1 for comparison.

surface is fractal, only to a shift of the data with respect to the axes on a vector of slope equal to -1.

The results of the full analysis of rod 3 of IFA-558 are shown in Fig. 9 along with the coefficients obtained from the conventional analysis of Eq. (4). The two lower traces show the fuel rod power history and the measured fuel centre temperature. The conventional analysis is displayed in the third trace and the recoil and slope components are observed to increase following the breach of the fission gas release threshold – i.e. the dashed line in the second trace. Note that the increases in the two components of the conventional analysis follow the same trend, similar to the behaviour in the IFA-430 slow-ramp in Fig. 4 but over a much extended time scale.

The upper trace shows the fractal analysis and this provides a far sharper definition of the transition to interlinkage than the conventional recoil plus slope approach. The main reason for this stems from the fact that the box-counting dimension, D_B, remains essentially constant with irradiation. There might be a slight increase in magnitude with burn-up but this is small compared with the large changes in the pseudo-fractal S/V. In contrast, the conventional analysis exhibits comparable changes to both the recoil and the diffusional slope components thus any change is spread over two variables whereas in the fractal analysis it is essentially concentrated into the one single change, that is, the change in the effective fractal surface-to-volume ratio. There is, of course, a residual amount of recoil release, as indeed, there must be, but in these cases there is no increase in recoil, or lambda-independent release with burn-up. What was erroneously interpreted as lambda-independent release, was, in fact, enhanced diffusion from the surface layers made more evident by the increase in the S/V. The lack of any large changes in the box-counting dimension, D_B, suggests that the newly

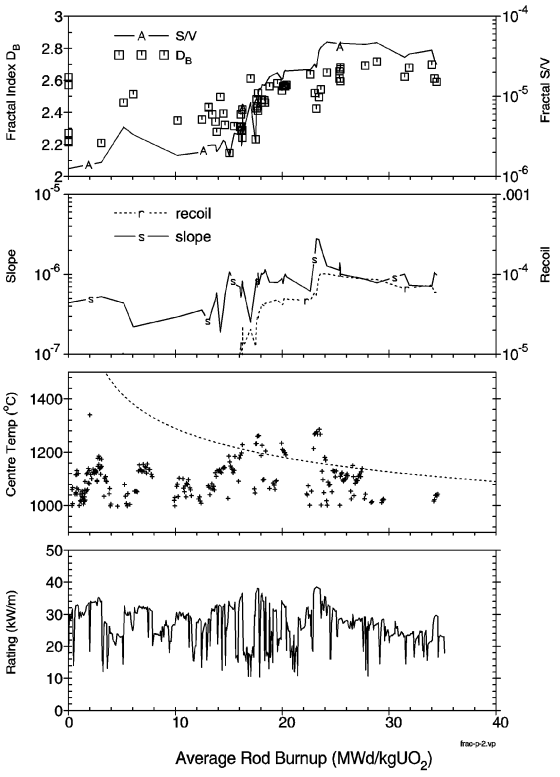

Fig. 9. The two lower traces show the power and temperature history of rod 3 in IFA-558. The dotted line in the second trace is the fission gas release threshold. The third trace shows the conventional analysis of diffusion (slope) and recoil – see Eq. (4). Note that both of these components appear to increase following the breach of the fission gas release threshold at around 16 MWd/kgUO$_2$. The results of the fractal analysis are displayed in the upper trace. The symbols represent the box-counting dimension or fractal index. Values greater than 2 imply fractal behaviour. The solid line is the pseudo-fractal S/V and exhibits much more dramatic post-interlinkage behaviour than the conventional analysis.

revealed surfaces exposed during interlinkage possess the same degree of fractal self-similarity as the exposed surfaces at the start of life. Any slight increase in this index could indicate that the self-similarity is increasing with burn-up and this might be a result of surface disruption caused by exiting recoiled fission fragments but the effect is clearly small.

4.4. The diffusion coefficient for short-lived fission products

Although absolute values of the diffusion coefficient cannot be ascertained from gas flow rig data, the trends with rod-average temperature and rating can be determined. By scaling the diffusional slopes to coincide with

the Turnbull correlation [2,3] at some arbitrary temperature, the trends with rating and temperature can be estimated albeit within the limitations imposed by the temperature averaging process.

The slow-ramp performed in IFA-430 provided a large amount of high quality data and an analysis based on conventional diffusion yielded values of diffusion coefficients of similar rating and temperature dependence to those in Eq. (1). However, examination of Figs. 2 and 4 reveals that there was possibly a weak temperature dependence as well as a rating dependence. A fractal analysis of the same data provides an ideal test of both the fractal model and the rating and temperature dependence of the fission gas diffusion coefficient.

In the conventional analysis – see Fig. 4 – the lambda-independent component was of the order of 3×10^{-4} but the expected contribution from true recoils would be in the range $2–4 \times 10^{-5}$ at the measurement pressure of 10 bar helium – see Fig. 3. The pseudo-fractal S/V was calculated from

$$\left.\frac{S}{V}\right|_{\substack{\text{pseudo}\\ \text{fractal}}} = \frac{R/B|_{\text{meas}} - R/B|_{\text{recoil}}}{\delta_{\text{p}}}, \tag{14}$$

where δ_{p} is defined in Eq. (11) and the recoil release component is set at 2×10^{-5}. Initially each dataset was fitted to Eq. (12) to establish the box-counting dimension, D_{B}. For the forty-seven datasets, the following result was obtained:

$$D_{\text{B}} = 2.45 \pm 0.13. \tag{15}$$

This demonstrates the fractal nature of the dataset. A value of 2.0 would indicate that the UO_2 surface was topologically smooth while a value of less than 2.1 or 2.2 might suggest that a more judicious choice of recoil component would have yielded a value of 2.0. The value given above plus the very small standard deviation provides strong evidence that the surface is indeed fractal rather than topologically smooth.

The next stage of the analysis involved refitting the entire dataset with a fixed value of D_{B}. The IFA-558 data in Fig. 9 indicate that D_{B} might change with irradiation, possibly through the creation of additional fractal surfaces in the exit wounds left by recoiling fission fragments. This process is on a much slower scale than the IFA-430 slow-ramp reported here so it is unlikely that D_{B} would actually change during the IFA-430 test. The value chosen for D_{B} was rounded up to 2.5, which although slightly larger than the value reported above, is, nevertheless, within half a standard deviation. The results of this analysis are reported in Fig. 10 in the same format as the conventional diffusional analysis presented in Fig. 4. The discrete symbols represent the pre-exponent, S_{PF} and the dashed line shows the trend expected from the Turnbull three-term diffusion coefficient. Eq. (12) predicts S_{PF} should vary as

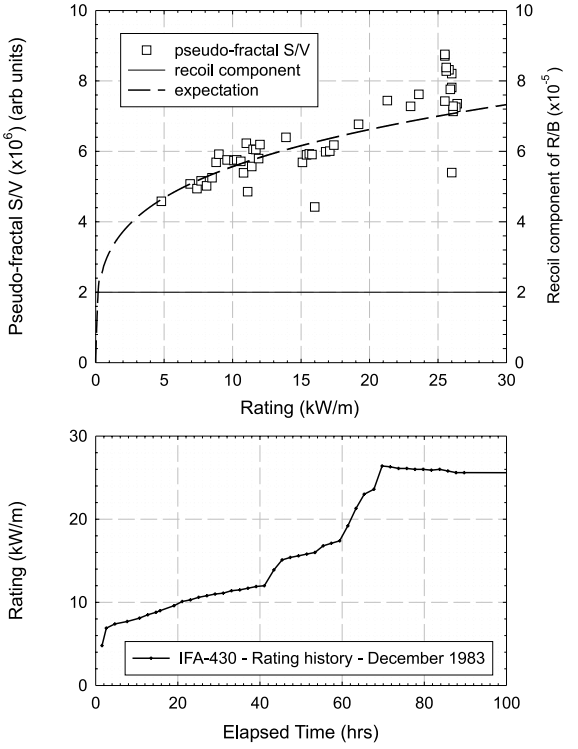

Fig. 10. A reanalysis of the slow-ramp in IFA-430 using fractal methods. The lambda-independent component has been set at 2×10^{-5}. Note the good agreement between the measured fractal S/V and the expectations based on D_3 proportional to rating compared to the conventional analysis in Fig. 4.

$D^{1/4}$ with a value of $D_{\text{B}} = 2.5$, i.e. $D_{\text{B}}^{(D-2)/2}$, and this appears to fit the results very well. It should be emphasised that the analysis was performed with a very low value of recoil release so the major component of release can be accounted for by diffusion through a fractal surface. In contrast, the major component of release using the conventional analysis in Fig. 4 was an assumed lambda-independent component of uncertain origin.

The good agreement with a diffusion coefficient varying linearly with rating should be contrasted with the conventional analysis of Fig. 4 where the measurements fall well below expectations at the lowest powers. This discrepancy had always been interpreted as evidence that the athermal term was temperature-dependent [27] but Fig. 10 indicates that proper treatment of the UO_2 surface removes the anomaly.

The rating dependence of the diffusion coefficient obtained from this test and other similar tests is shown in Fig. 11 confirming the good agreement with the D_3 term in Eq. (1). Also shown in this figure are the results from the conventional analysis showing the poor agreement at low powers.

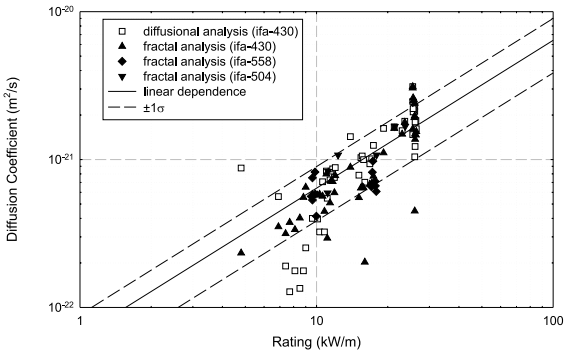

Fig. 11. Diffusion coefficients obtained by fractal analysis for IFA-430, IFA-504 and IFA-558 are shown as closed symbols. The values derived from the conventional analysis of IFA-430 are also shown for comparison as open symbols.

Finally, Fig. 12 shows the entire dataset from the IFA-430 slow-ramp plotted in true fractal form using the three-term diffusion coefficient from Eq. (1) along with the calculated rod-average temperatures. In this case the S/V axis represents the true surface-to-volume ratio appropriate to the mean-diffusion distance. The agreement with the slope of −0.5, that is, $D_B = 2.5$, over nearly two orders of magnitude change in the mean-diffusion distance is remarkable confirmation of the validity of the fractal approach for short-lived fission products with half-lives varying from 32 s (^{90}Kr) to 4.45 h (^{85m}Kr).

In the limit, the mean-diffusion distance for the short-lived fission products is around 0.1 nm which is a little less than the lattice spacing in UO_2. Fig. 7 shows that the mean-diffusion distance is associated with surface irregularities between five and ten times its own value indicating several lattice spacings. This is probably the lower limit for the mean-diffusion distance although it is certainly not meaningless since although the minimum jump distance is one lattice spacing, diffusion is a random process involving many fission gas atoms, say 10^{18}–10^{20} m^{-3}. There is no physical requirement that an atom should jump; some will jump, some will decay without jumping but on average the mean distance travelled in the fission product's lifetime will be the mean-diffusion distance and there is no stipulation that this is restricted to multiples of the lattice spacing. There is, however, a limitation of the scale of the surface irregularities so the value of 0.1 nm probably defines a lower meaningful limit.

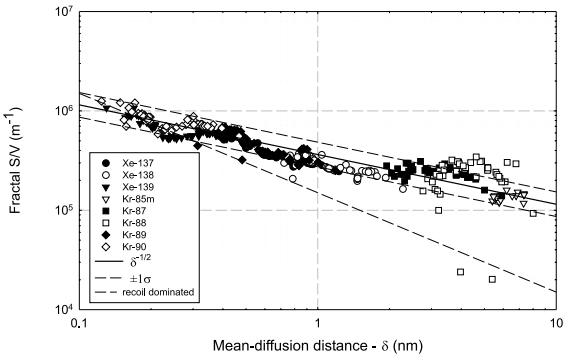

Fig. 12. True fractal plot for all data from the slow-ramp in IFA-430. The S/V ratios and mean-diffusion distances have been calculated using the three-term diffusion coefficient. Data from forty-seven spectra including 335 fission product release rate determinations are included in this figure.

Further examination of Fig. 12 reveals that at this lowest value the actual trend may be increasing from a slope of −1/2 to −1. This latter behaviour is symptomatic of a residual amount of true recoil release. So any inaccuracy in estimating the recoil release in the calculation of Eq. (14) will eventually lead to a linear tendency at the lowest values of δ. In this case the consequences are irrelevant because the fractal behaviour is well defined over the rest of the range.

4.5. Consequences for longer-lived fission product releases

Long mean-diffusion distances can result from large diffusion coefficients or long half-lives or both. The data in Fig. 12 were obtained from flow spectrometry on the integral fuel rod, IFA-430, so the average temperatures are such that the mean free paths never exceed 8 nm. At some point the S/V versus mean-diffusion distance curve should show a tendency to flatten indicating a transition to classical diffusional release from a topologically smooth surface. It is in this region that the release from the longer-lived and stable fission gas should occur. In order to explore this region it is necessary to increase the temperature and hence the diffusion coefficient.

IFA-563 [27] utilised thin wafers of UO_2 sandwiched between molybdenum discs in order to provide more uniform temperatures and more accurately represent isothermal conditions. A staircase start-up ramp was employed and gas release measurements were obtained with helium and argon sweep gas. Argon has a much poorer thermal conductivity than helium so the fuel operated at higher temperatures. The experiment provided data at two separate temperatures for each heat rating in an attempt to de-couple the rating and temperature dependences. A slight complication in the tests resulted in a higher than expected contribution from recoil, particularly in the argon swept rod. However, despite this, the results are highly instructive. In Fig. 13, the data from a helium-swept rod are shown. At low values of mean-diffusion distance the behaviour is dominated by the presence of recoils but fractal behaviour is clearly evident and persists up to the highest values achieved in the experiment, that is, around 40 nm.

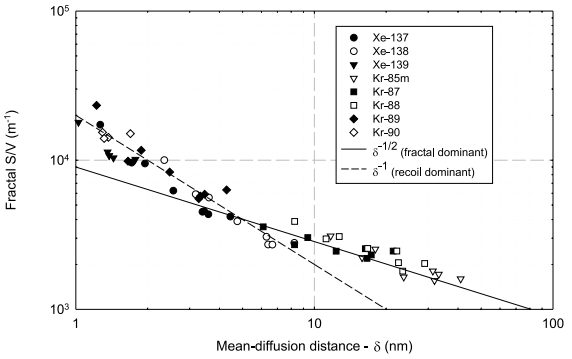

Fig. 13. True fractal plot for rod 10 of IFA-563 using helium sweep gas. Note the tendency for the slope to increase to −1 as a result of residual recoils. There is no tendency for the S/V to level off at large mean-diffusion distances before a value of 40 nm.

In contrast, Fig. 14 shows the effects with argon fill gas. In this case there seems to be little or no fractal behaviour and the data could have been analysed using the standard recoil plus slope method of Eqs. (3) and (4).

From these two figures it could be inferred that the transition to classical behaviour takes place when the mean-diffusion distance is somewhere between 40 and 70 nm. For mean-diffusion distances greater than this value, the S/V appears to be constant. This is possibly the reason for the discrepancy between the values of diffusion coefficient measured for short- and long-lived fission products. In these tests, the Turnbull [2,3] diffusion coefficient was used to obtain values of S/V which were then used to evaluate the diffusivity of the longer-lived product. It must be assumed that a better estimate of the long-lived fission product diffusivity would have been

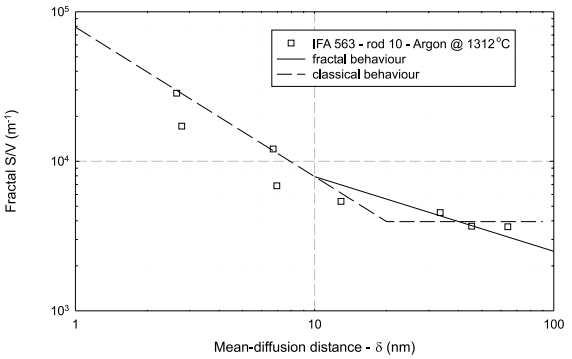

Fig. 14. True fractal plot for rod 10 of IFA-563 using argon sweep gas. The trend is for a direct move from recoil to conventional diffusional release behaviour with no fractal behaviour evident. The transition presumably takes place at mean-diffusion distances between the upper points on Fig. 13 and those in this figure.

obtained if a value of S/V more appropriate to its own mean-diffusion distance had been used.

Corrections to the diffusion coefficients of longer-lived fission products shown in Fig. 2 can be made by using the scheme summarised in Fig. 15. The solid line shows the true behaviour of the fractal S/V based on a D_B value of 2.5. The experimental situation was as follows:

1. Short-lived fission product measurements were performed on the fuel at a certain temperature and rating and yielded a value of S/V. The measurements will have been performed over a range of values of mean-diffusion distances but it is convenient to assume that the reference value, δ_{ref} corresponds to that of the longest-lived isotope; usually this will be ^{85m}Kr, with a half-life of 4.45 h.
2. The release rates of the longer-lived fission products were measured by cold-trapping techniques.
3. The mean-diffusion distances of the products are evaluated at δ_A and δ_B using the same diffusivity as that used for the ^{85m}Kr evaluation.
4. The diffusivities of the two products are estimated using the S/V evaluated for ^{85m}Kr as D^A_{est} and D^B_{est}, respectively.

It is straightforward to demonstrate that the corrected values of diffusivity of these products may be obtained from

$$D^A_{correct} = D^A_{est}\frac{\delta_A}{\delta_{ref}}$$

and (16)

$$D^B_{correct} = D^B_{est}\frac{\delta_{trans}}{\delta_{ref}}.$$

This method has been used to correct the diffusivities of the longer-lived products. It can be seen in Fig. 2 that there are a number of cases where the discrepancy is too large to be accounted for and these cases have been excluded from the optimisation exercise. The forty-eight separate measurements of ^{131}I, ^{131m}Xe, ^{133}Xe and ^{85} Kr

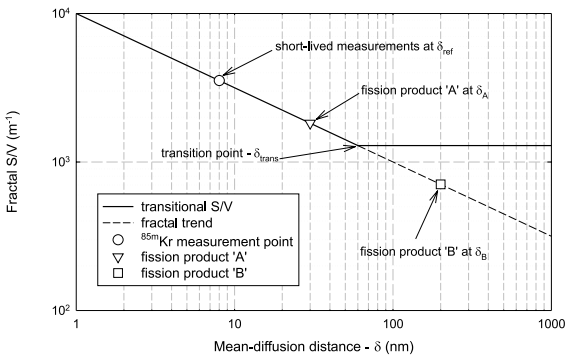

Fig. 15. Schematic diagram showing how long-lived diffusion coefficients may be corrected for the fractal change in S/V.

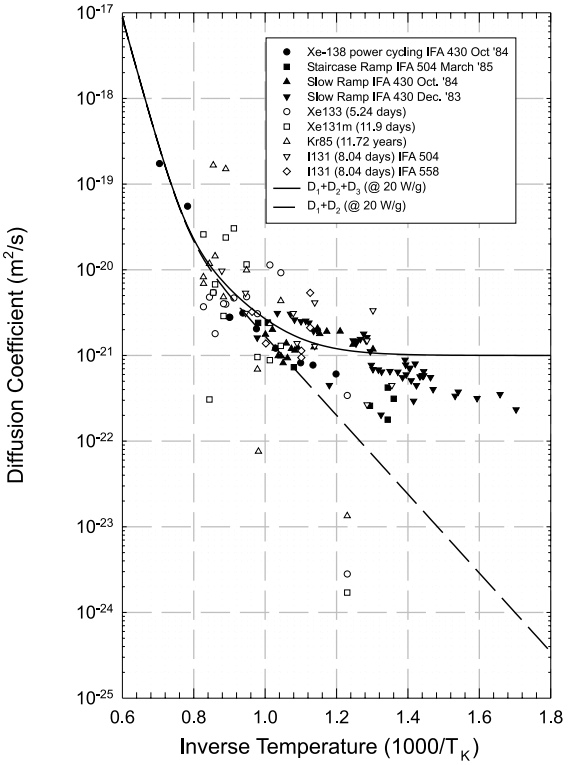

Fig. 16. Diffusion coefficient plot with values recalculated from fractal analysis. Most of the long-lived data now sit on the three-term line. Note that the solid lines were calculated at fixed values of rating whereas the data at the lowest temperatures were not at fixed rating.

have been corrected using Eq. (16) and the optimum value of δ_{trans} is between 45 and 65 nm with an average of 57 nm. This value is consistent with the data in Figs. 13 and 14 and the corrected values of diffusivity are plotted in Fig. 16.

5. Discussion

The release of both short- and long-lived fission products from irradiated UO_2 may be understood on the basis of diffusion from a solid bounded by a fractal surface. The fractal nature is defined in terms of the mean-diffusion distance of the radioactive fission products and the effective S/V increases as the mean-diffusion distance decreases. The degree of fractality is defined by the box-counting dimension, D_B, which in the cases considered here has a value of around 2.5. Whether or not this value is characteristic of all UO_2 is not presently known but it would appear that the value might increase slightly with burn-up, possibly as a result of surface disruption caused by recoiling fission fragments.

Any value of D_B greater than the topological dimension of a surface, i.e. 2, indicates that the surface is fractal although values less than 2.2 would be less convincing; the values observed for IFA-430, IFA-558 and IFA-563 are unequivocal in this respect.

The question arises as to the origin of the fractal behaviour. In part this must stem from the initial crystallisation of the solid during manufacture although there will undoubtedly be a contribution from the newly exposed fracture surfaces created during the initial rise to power. The development of the S/V during the interlinkage stage of IFA-558 shown in Fig. 9 suggests that the newly exposed surfaces are also fractal but it is not clear whether this is of fundamental crystallographic origin or arising from surface disruption by recoils. At some stage these surfaces would have been closed grain boundaries and have become exposed by the growth and interconnection of fission gas porosity. It might be imagined that any surface irregularities would be rapidly smoothed by capillarity driven surface diffusion [28] but at the low temperatures of these tests the diffusion rates may be slow compared to the surface exposure rates. The disruptive effects of recoils leaving the fuel surface would undoubtedly cause the generation of new fractal surfaces and these probably form more rapidly than surface diffusion can heal them. It is possible that as the fuel temperatures increase, the fractal nature might disappear but this effect would be masked by the fact that the fission gas diffusion rates would also increase, shifting the diffusion into the classical regime above δ_{trans}. It is an interesting possibility that if surface smoothing occurs during a high temperature transient, the subsequent behaviour during return to normal operations might be characterised by a temporarily reduced value of D_B.

The introduction of the fractal interpretation leads to a simplification in the understanding of the radioactive fission product release. No sensible physical reasons had ever been advanced for the apparent differences in diffusion rates of short- and long-lived products, and the use of different values was employed purely as an engineering criterion without any underlying physical rigour. The previous use of a uniform value of S/V regardless of fission product mean-diffusion distances also led to the inconvenient emergence of an additional component of recoil or lambda-independent release. This term disappears when a fractal interpretation is used although a residual, and physically understandable, recoil component remains.

The fractal behaviour of the surface is manifested over a large range of mean-diffusion distances. At the low end the behaviour is terminated when the mean-diffusion distance is of the order or less than the lattice spacing. Since the surface irregularities are of the order

of five or ten times larger than the mean-diffusion distance this is an understandable result. Classical behaviour characterised by release from a topologically smooth surface is estimated to resume when the mean-diffusion distance exceeds a value of approximately 60 nm. For fission products with mean-diffusion distances greater than this transitional value the surface appears to have a constant value of S/V defined by the macroscopic dimensions. This will always embrace isotopes such as ^{85}Kr with a 10.72-year half-life and the stable fission gases. For all other isotopes the mean-diffusion distance depends on the diffusion coefficient and hence the temperature. The release of ^{133}Xe isotope with a 5.24-day half-life becomes classical when the diffusion coefficient exceeds 5.5×10^{-21} m^2/s; this occurs at the relatively low temperature of 875°C. It is highly probable that all examples of transient release of this isotope following the rapid venting of grain boundaries occur under classical release conditions. This will also be the case for ^{131}I with an 8.04-day half-life. The measurements, on which the diffusion coefficient estimates reported in Figs. 2 and 16 were based, were made on fuel at relatively low temperatures. Transition to classical behaviour occurs for this isotope at around 810°C so no particular benefits can be claimed for release from fractal surfaces because the fuel surface area under any conceivable fault scenario will have ceased to fall as rapidly as in the fractal regime.

When the diffusion coefficient anomaly was first reported [15], it was suggested that the D_3 component might be a near-surface effect. The use of a fractal interpretation renders the supposition irrelevant and possibly untestable. The results from the two-zone simulation in Section 3 show that in the region where the inner-zone diffusion coefficient is small, the release tends to be dominated by the outer-zone. At higher temperatures the diffusivities of the two-zones are convergent and larger than the D_3 term. So the release is dominated by a term in $D_1 + D_2$ which far exceeds D_3 anyway.

6. Conclusions

An analysis of selected gas flow rig data has been performed using standard fractal methods. The assumptions implicit in this approach are that the surface of UO_2 is self-similar in possessing surface irregularities at all levels of magnification and that the diffusion distance of short-lived fission products from birth to decay is a suitable measuring rod with which to define the self-similarity. On the basis of the analysis of data from the Halden Project assemblies IFA-430, IFA-504, IFA-558 and IFA-563, it is concluded that:

1. The apparently anomalous behaviour of short- and long-lived fission products is not a product of any near-surface diffusion enhancement effect. These effects would always produce opposite effects to those expected of them, i.e. the diffusional releases of long- and short-lived products should converge at low temperatures rather than diverge.
2. The surface of UO_2 shows a strong degree of self-similarity defined by fractal box-counting dimensions of around 2.5 with the self-similarity persisting down to near-atomic spacing dimensions. At large diffusion distances the surface-to-volume ratio appears to become constant at a low value defined by its macroscopic dimensions.
3. The transition from fractal to classical behaviour occurs for mean-diffusion distances around 60 nm.
4. The release of all fission products whether short-lived, long-lived or stable can be described by the three-term diffusion coefficient.
5. There is no burn-up enhancement of the lambda-independent release. The observed effects are a product of enhanced diffusional release from large S/V ratios existing at short diffusion distances. The enhancement of the short-lived products over the long-lived products is a result of the fractal self-similarity of the surface.

Acknowledgements

I dedicate this paper to the memory of Richard White who recognised the beauty of fractals long before I recognised their value.

References

[1] C. Vitanza, E. Kolstad, V. Graziani, in: Proceedings of ANS Topical Meeting on LWR Fuel Performance, Portland, OR, USA, ANS, La Grange Park, IL, 1979, p. 366.
[2] J.A. Turnbull, C.A. Friskney, J.R. Findlay, F.A. Johnson, A.J. Walter, J. Nucl. Mater. 107 (1982) 168.
[3] J.A. Turnbull, R.J. White, C. Wise, The diffusion coefficient for fission gas atoms in uranium dioxide, in: Proceedings of the IAEA Technical Committee Meeting on Water Reactor Fuel Element Computer Modelling in Steady-State, Transient and Accident Conditions, Preston, UK, 1988, IAEA-TC-659/3.5, p. 174.
[4] D. Davies, G. Long, Report AERE 4347, 1963.
[5] Hj. Matzke, J. Phys. Colloq. (Suppl. 34) (1973) C9.
[6] R.J. White, E. Skattum, A. Haaland, I.D. Palmer, Review of fission product release measurements from fuel irradiated in the gas flow rigs 1980–1985, Halden Project, HPR 326, June 1985.
[7] A.H. Booth, A method for calculating the diffusion of radioactive rare gas fission products from UO_2 fuel elements, AECL Chalk River, Report DCI-27, 1957.
[8] J.A. Turnbull, J. Gratton, G. Smith, D.A. Cordall, R.M. Cornell, Measurement of ^{85}Kr as a method of assessing fission gas release in CAGR fuel pins, in: Proceedings of

the BNES Conference on Nuclear Fuel Performance, Stratford-on-Avon, UK, 1985, p. 319.
[9] P.A. Tempest, The reliability of on-line fission gas release measurements in the study of fuel interlinkage and resintering phenomena, HWR 275, 1991.
[10] T.S. Noggle, J.O. Stiegler, J. Appl. Phys. 31 (1960) 2199.
[11] C.A. Friskney, M.V. Speight, J. Nucl. Mater. 62 (1976) 89.
[12] R. Hargreaves, D.A. Collins, J. Br. Nucl. Energy Soc. 15 (1976) 311.
[13] P.A. Tempest, E. Skattum, A. Haaland, Fission gas release during stepped power increases in the gas flow rig above 15 MWd/kgUO_2, HWR 258, 1990.
[14] A.H. Booth, A method of calculating fission gas diffusion from UO_2 fuel and its application to the X-2-f loop test, Report AECL 496, 1957.
[15] R.J. White, J.A. Turnbull, A.D. Appelhans, E. Skattum, A. Haaland, The release of ^{85}Kr in the gas flow rig IFA-504, Halden Project IDG Note 2951, 1984.
[16] R.J. White, E. Skattum, A. Haaland, The communication of fission products in the interior of a fuel rod with particular emphasis on recent tests on the IFA-430 gas flow rig, HPR 325, 1985.
[17] C. Baker, J. Nucl. Mater. 66 (1977) 283.
[18] J.A. Turnbull, J. Nucl. Mater. 38 (1971) 203.
[19] M.V. Speight, Nucl. Sci. Eng. 6 (1969) 180.
[20] C. Baker, R. Corcoran, A.T. Donaldson, R.J. White, An investigation of the intra-granular fission gas bubble distributions in CAGR fuel following power ramps in the Halden reactor, Paper Presented at the EHPG, Loen, Norway, May 1996.
[21] R.J. White, The growth of intra-granular bubbles in post-irradiation annealed UO_2 fuel, in: Proceedings of the IAEA Technical Committee on Nuclear Fuel Behaviour Modelling at High Burn-Up and its Experimental Support, Lake Windermere, UK, June 2000 (in press).
[22] R.J. White, A. Haaland, E. Skattum, The power and burn-up dependence of thermal and fission product release phenomena deduced from fuel irradiated in the gas flow rigs IFA-430 and IFA-504, HWR 119, 1984.
[23] R.J. White, M.O. Tucker, J. Nucl. Mater. 118 (1983) 1.
[24] M. Schroeder, Fractals, Chaos, Power Laws, Minutes from an Infinite Paradise, W H Freeman and Company, New York, ISBN 0-7167-2136-8, 1991.
[25] R. Rucker, Infinity and the Mind, The Science and Philosophy of the Infinite, Princeton University, ISBN 0-14-026295-4, 1995.
[26] P.S. Addison, Fractals and Chaos, An Illustrated Course, Institute of Physics Publishing, Bristol, ISBN 0-7503-0399, 1997.
[27] R.J. White, P.A. Tempest, P. Wood, An evaluation of diffusion coefficient data obtained from the start-up ramp of IFA-563 and comparison with data from the gas flow rigs IFA-504 and IFA-558. Paper presented at the EHPG, Storefjell, Gol, Norway, 1993.
[28] W.M. Mullins, J. Appl. Phys. 30 (1959) 77.